Lawrence Berkeley Laboratory
UNIVERSITY OF CALIFORNIA

Accelerator & Fusion Research Division

Submitted to Review of Scientific Instruments

REAL TIME DIGITAL SPECTRAL ANALYSIS AS A PLASMA FLUCTUATION DIAGNOSTIC

Kurt F. Schoenberg

October 1979

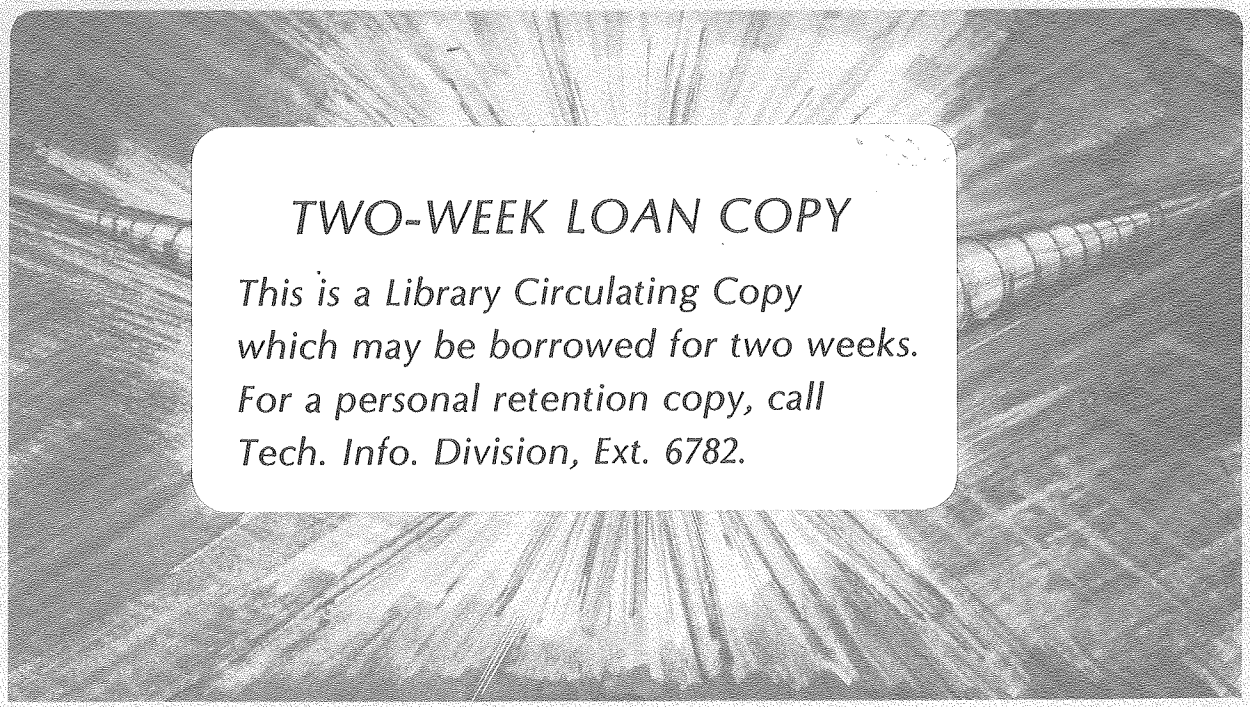

Prepared for the U.S. Department of Energy under Contract W-7405-ENG-48

DISCLAIMER

REAL TIME DIGITAL SPECTRAL ANALYSIS AS A PLASMA FLUCTUATION DIAGNOSTIC

Kurt F. Schoenberg†
Lawrence Berkeley Laboratory
University of California
Berkeley, California 94720

ABSTRACT

A real time digital spectral analysis system, applicable to broad band plasma fluctuations, is presented. The system digitally records plasma potential fluctuations on a pair of matched electrostatic probes, and subsequently outputs the cross power spectral density and phase via an on-line computer graphics display. The spectral analysis system and its experimental accuracy are discussed. Using the Lawrence Berkeley Laboratory ten amp neutral beam ion source, several examples demonstrating the systems application to plasma wave detection are given.

INTRODUCTION

Temporal signal processing techniques are widely employed in plasma physics to investigate plasma waves, instabilities and turbulence. For example, experimental knowledge of the spatial and temporal dependence of plasma fluctuations is necessary in order to study their relationship with anomalous transport or non-linear phenomena.[1-12] Historically, early temporal techniques were primarily limited to analog measurement of the two-time correlation function. Although correlation techniques were experimentally effective, they required measurement over a narrow bandwidth.[1,3,11] Wideband fluctuation analysis was therefore a fairly laborious process involving extensive analog filtering and measurement iteration.

An equivalent, but ofttimes more transparent method of fluctuation analysis involves power spectrum measurement. The power spectrum is essentially a Fourier transform of the correlation function, and is equivalent to the correlation function in information content. However, it provides an additional advantage that fluctuation phenomena are described in the frequency domain, which for many applications is advantageous over the time domain correlation format (e.g., the study of plasma dispersion characteristics or the spectral index and mode coupling properties of turbulent plasmas). In addition, recent advances in digital electronics, and the development of a fast Fourier transform (FFT) algorithm[13-17] have greatly facilitated both the speed and accuracy of power spectral acquisition and analysis; allowing broadband measurement with minimal analog filtering. This paper presents the digital spec-

tral analysis system used to study ion acoustic fluctuations in the LBL 10 ampere neutral beam ion source.

I. THEORY OF MEASUREMENT

Let $\phi_A(t)$ represent a general time dependent signal describing some intensive property of a physical system. For example, $\phi_A(t)$ may represent the fluctuating electrostatic potential in a plasma. Apart from the mean averaged signal power, the simplest nontrivial function describing the temporal characteristics of $\phi_A(t)$ is the two-time correlation function:[18]

$$C_{AA}^{\phi}(\tau) = \langle \phi_A(t)\phi_A(t-\tau)\rangle_t = \lim_{T\to\infty} \frac{1}{2T}\int_{-T}^{T} \phi_A(t)\phi_A(t-\tau)dt \qquad (1)$$

where T represents the total signal observation time. Mathematically, the correlation function is a real and even function of τ; conditions which result from constraints of reality and the time invariant nature of the physical processes which drive $\phi_A(t)$. Despite its adjudged simplicity, the correlation function contains an appreciable amount of information about the statistical properties of $\phi_A(t)$. It is, in essence, a measure of the dependence between the physical processes driving $\phi_A(t)$ at different times (i.e., a measure of the systems temporal memory) and in this sense, describes its time variation.[19]

An alternate but equivalent description of the correlation function in the frequency domain is given by the auto power spectral density function:

$$S^{\phi}_{AA}(\omega) = \lim_{T\to\infty}\left[\frac{\phi^{*}_{A}(\omega)\,\phi_{A}(\omega)}{T}\right] = \int_{-\infty}^{\infty} C^{\phi}_{AA}(\tau)e^{i\omega\tau}d\tau \qquad (2)$$

where:

$$\phi_{A}(\omega) = \int_{-\infty}^{\infty} \phi_{A}(t)e^{i\omega t}dt$$

$$\phi_{A}(t) = \frac{1}{2\pi}\int_{-\infty}^{\infty} \phi_{A}(\omega)e^{-i\omega t}d\omega \qquad (3)$$

and where $S^{\phi}_{AA}(\omega)$ is a real, even and non-negative function of ω. The inverse transform of equation 2 returns the correlation function:

$$C^{\phi}_{AA}(\tau) = \frac{1}{2\pi}\int_{-\infty}^{\infty} S^{\phi}_{AA}(\omega)e^{-i\omega t}d\omega \qquad (4)$$

Equations 2 and 4 are formally recognized as the Weiner-Khintchine relations which illustrate the equivalence between a correlation and power spectral density description of fluctuation phenomena. Combining equations 1 and 4 for the case of $\tau = 0$ yields the power balance condition:

$$\langle(\phi_{A}(t))^{2}\rangle_{t} = C_{AA}(0) = \frac{1}{\pi}\int_{0}^{\infty} S^{\phi}_{AA}(\omega)d\omega \qquad (5)$$

which physically states that the mean squared signal power must equal the total integrated power spectral density. Equation 5 thus provides a convenient and reliable method of checking the accuracy and validity of experimental power spectrum measurements.

The generalization from one to two signal sample points is rather straightforward. Given two signals $\phi_A(\vec{x}_A,t)$ and $\phi_B(\vec{x}_B,t)$, again possibly representing the electrostatic potential fluctuation at two spatial locations in a plasma, the two-point, two-time cross correlation function is defined by:

$$C^{\phi}_{AB}(\vec{R},\tau) = \lim_{\substack{T\to\infty \\ V\to\infty}} \frac{1}{2TV} \int_{-T}^{T}\int_{V} \phi_A(\vec{x}_A,t)\phi_B(\vec{x}_A-\vec{R},t-\tau)d\vec{R}d\tau \qquad (6)$$

where:

$$\vec{R} = \vec{x}_A - \vec{x}_B$$

The corresponding cross power spectrum is therefore:

$$\begin{aligned} S^{\phi}_{AB}(\vec{k},\omega) &= \int_{-\infty}^{\infty}\int_{-\infty}^{\infty} C^{\phi}_{AB}(\vec{R},\tau)e^{i(\omega\tau-\vec{k}\cdot\vec{R})}d\tau d\vec{R} \\ &= \lim_{T,V\to\infty}\left\{\frac{\phi^*_A(\vec{k},\omega)\phi_B(\vec{k},\omega)}{T\ V}\right\} \end{aligned} \qquad (7)$$

Experimentally, $S(\vec{k},\omega)$ contains a reasonably complete description of the spatial and temporal characteristics of fluctuations within the physical system. However, it is often unnecessary to measure the full spatial content of $S(\vec{k},\omega)$ in order to draw relevant physical conclusions from the analyzed data. For example, if plasma potential fluctuations result from the excitation of a unidirectionally propagating normal plasma mode, then within the limitations imposed by linear theory, they can be described in terms of a superposition of monochromatic plane waves:

$$\phi(\vec{x},t) = \int_{-\infty}^{\infty} \alpha(\omega) e^{-i(\omega t - \vec{k}(\omega)\cdot\vec{x})} d\omega \qquad (8)$$

where $\vec{k}(\omega)$ is a solution of the linear mode dispersion relation and $\alpha(\omega)$ describes the frequency dependent wave amplitude function. For this case, a complete description of the cross power spectrum (equation 7) is obtainable by measuring the spectral function:

$$S_{AB}^{\phi}(\vec{R},\omega) = \int_{-\infty}^{\infty} C_{AB}^{\phi}(\vec{R},\tau) e^{i\omega\tau} d\tau \qquad (9)$$

$$= \lim_{T\to\infty} \left[\frac{\Phi_A^*(\vec{x}_A,\omega)\Phi_B(\vec{x}_B,\omega)}{T} \right]$$

which is experimentally expeditious since analysis does not require the computation of a spatial Fourier transform and hence, in principle, only two spatial samples are necessary. Fourier transforming equation 8 and substituting into (9) yields:

$$S_{AB}^{\phi}(\vec{R},\omega) = |S_{AB}^{\phi}(\omega)| e^{i\Theta_{AB}(\vec{R},\omega)} \qquad (10)$$

where

$$|S_{AB}^{\phi}(\omega)| = \lim_{T\to\infty} \left[(1/T) |\alpha_A^*(\omega)\ \alpha_B(\omega)| \right] \qquad (11)$$

and

$$\Theta_{AB}(\vec{R},\omega) = [\Theta_B(\vec{x}_B,\omega) - \Theta_A(\vec{x}_A,\omega)] = \vec{k}(\omega)\cdot\vec{R} \qquad (12)$$

The cross power spectral density, $|S_{AB}^{\phi}(\omega)|$, is a physical measure of the coherence between temporal fluctuations occurring at sample points A and B. In analogy with optics, a normalized version of $|S_{AB}^{\phi}(\omega)|$

called the spectral coherence function, is defined by:

$$\gamma^{\phi}_{AB}(\omega) = \frac{|S^{\phi}_{AB}(\omega)|}{[S^{\phi}_{AA}(\omega)S^{\phi}_{BB}(\omega)]^{1/2}} \tag{13}$$

where $S^{\phi}_{AA}(\omega)$ and $S^{\phi}_{BB}(\omega)$ are the auto power spectral density at points A and B respectively. In essence, $\gamma^{\phi}_{AB}(\omega)$ is the normalized cross power spectral density $(0 \leqslant \gamma^{\phi}_{AB}(\omega) \leqslant 1)$ where low (high) values within a particular bandwidth imply incoherence (coherence) between fluctuations at the sample points. The cross power phase spectrum, $\Theta_{AB}(\vec{R},\omega)$, is defined as the relative spectral phase difference between fluctuations at the sample points and is therefore a measure of the plasma dispersion relation $(k(\omega))$.

Equations 9 through 13 illustrate that under the assumption of normal mode excitation (equation 8), the general cross power spectrum can be obtained by two fixed sample points with arbitrary non-zero separation. The inclusion of wave damping adds the additional constraint that sample point separation must remain less than the wave spatial coherence length. Mathematically, this simplified description results from the well-defined relationship between ω and $\vec{k}$ as defined by the linear dispersion relation, and can be illustrated by spatially transforming equation 10 to obtain the general cross power spectrum:

$$S^{\phi}_{AB}(\vec{k},\omega) = \int_{-\infty}^{\infty} S^{\phi}_{AB}(\vec{R},\omega)e^{-i\vec{k}\cdot\vec{R}}d\vec{R} = |S^{\phi}_{AB}(\omega)|\,\delta(\vec{k}-\vec{k}(\omega)) \tag{14}$$

Thus, in frequency bands where equation 14 is valid, the cross power spectrum will yield a high degree of coherence (equation 13) with the dispersion relation defined by equation 12. For cases where equation 14 is not valid,[20] the full cross power spectrum must be measured.

II. EXPERIMENTAL APPARATUS

A. Plasma Source

Figure 1 illustrates a cross-sectional schematic of the LBL ten ampere source which is basically a small version of the ion sources presently employed in the LBL/LLL neutral beam program.[21] The source produces a plasma via a diffuse, low pressure, high current electrical discharge. Arc ionization is produced by primary electrons originating at the thermionic cathode (filament ring), and energized by their passage through the cathode-plasma sheath. The arc discharge occurs between the filament ring, consisting of 26 hairpin filaments connected in parallel, and the anode ring. A pulse line composed of iron core inductors and electrolytic capacitors supplies roughly 10 to 60 kW of arc power for up to 100 msec. All source chamber walls electrically float at potentials such that the net random current due to electron and ion bombardment is nulled. The main volume of the discharge is relatively free of magnetic fields, although both filament heater current and arc discharge current contribute to a small field in the vicinity of the filaments. For this reason, the applied filament current is D.C. to minimize A.C. modulation of discharge conditions. To avoid formation of a substantial anode sheath, which increases discharge noise, the anode area is chosen such that the discharge arc current is supplied by the random electron flux striking the anode.

Experimental access to the plasma is via several radial probe ports near the source midplane and floating source grid, one axial probe port, and a section of axially symmetric floating wall which can be used as an extended wall probe.

B. Spectral Analysis System

Figure 2 schematically illustrates the digital spectral analysis system. Potential fluctuations are detected by two matched and shielded electrostatic probes, which are mounted on vernier drivers enabling probe separation adjustment while maintaining vacuum integrity. A set of external probe access ports allow axial, radial and azimuthal alignment for wave propagation measurements. The probe signals are processed through a matched pair of pass band filters, amplified and digitized by a Nicolet transient recorder; which is capable of 8 bit/ 50 nsec per point analog to digital conversion. Filter pass bands are set by requirements to suppress transient turn on and power supply noise (low frequency cut off) and to suppress aliasing effects (high frequency cut off). The digitized data is finally read by a Modcomp Systems computer over a direct I/O link, which subsequently executes a spectral analysis algorithm providing on-line analysis via a Tektronix 4014 graphics terminal. Disk and magnetic tape storage supply the capability for multiple data set averaging which is necessary in order to obtain low noise broadband power spectrum estimates. Hardcopy alpha-numeric and graphical output is provided by a Versatek printer/plotter.

The spectral analysis system is capable of power spectrum measurement over a 10MHz bandwidth with a spectral resolution of 2.5kHz, and fluctuation power levels down to $10^{-11}V^2/kHz$. Minimum power level

resolution is primarily set by input amplifier and digitization noise since shielding minimizes external RF pickup. System performance is periodically checked by using the power balance condition (equation 5) on a calibrated signal. Measured integrated power spectral density typically agrees with RMS signal power to within ten per cent.

Equation 12 demonstrates the importance of matching data acquisition channels in the detection apparatus. Since the cross power phase spectrum is dependent only on the relative phase between channels, proper matching insures minimal systematic measurement error. Measured phase error is typically less than .01 (0.1) radians over a 1(10)MHz bandwidth respectively.

III. ACCURACY ANALYSIS

The accuracy of the spectral analysis system is dependent on the response characteristics of the probe shielded cables, band pass filters and input amplifiers (Fig. 2); and the acquisition and numerical accuracy of the signal digitizer and spectral analysis algorithm. Pedagogically, these effects may be approximately modeled within the formalism of linear network theory where signal modification by detection system characteristics are described in terms of a frequency response function $H_{sys}(\omega)$. That is, given a time dependent signal $\phi(t)$ with spectral density $\Phi(\omega)$, the detected signal is:

$$\phi_{DET}(t) = \frac{1}{2\pi} \int_{-\infty}^{\infty} H_{sys}(\omega)\, \Phi(\omega) e^{-i\omega t}\, d\omega \qquad (15)$$

or equivalently:

$$\Phi_{DET}(\omega) = H_{sys}(\omega)\Phi(\omega) \tag{16}$$

In general, $H_{sys}(\omega)$ is a complex function whose real and imaginary components, describing detection system amplitude and phase response, are related via the Kramers-Kronig relations.[22]

In application to spectral analysis, the detected cross power spectral density (equation 9-11) of two signals ($\phi_A(\vec{x}_A,t)$, $\phi_B(\vec{x}_B,t)$) measured by two channels of a system with response ($H_A(\omega)$, $H_B(\omega)$) is:

$$S^{\phi}_{AB}(\vec{R},\omega)\Big|_{DET} = \lim_{T\to\infty}\left\{\frac{1}{T}\left|\Phi^*_A(\omega)H^*_A(\omega)\Phi_B(\omega)H_B(\omega)\right|e^{i[\Theta_{AB}(\vec{R},\omega)+\Theta_H(\omega)]}\right\} \tag{17}$$

where $\Theta_H(\omega)$ defines the system induced phase shift. If $H_A(\omega) = H_B(\omega) = H(\omega)$:

$$S^{\phi}_{AB}(\vec{R},\omega)\Big|_{DET} = \left|S_{AB}(\vec{R},\omega)\right|\left|H^2(\omega)\right|e^{i\Theta_{AB}(\vec{R},\omega)} \tag{18}$$

In theory, equation 17 or 18 can be digitally inverted to obtain the actual cross power spectrum if an accurate form of $H(\omega)$ is available.[23-25] However, it is experimentally wise to judiciously design the detection apparatus to minimize system induced effects over the measurement bandwidth. This requires signal channels be effectively matched in order to minimize phase error; and the modulus of the response function, $|H(\omega)|$, should remain reasonably flat across the desired cross power spectral bandwidth. Semi-quantitative knowledge of $H(\omega)$ is therefore important in order to provide a basis for reasonable experimental procedure and design.

A. Probe-Plasma and Analog Circuit Effects

Signal response of the spectral analysis system (Figure 2) can be effectively modeled by the schematic equivalent illustrated in Figure 3 (one channel). The schematic is composed of three conceptually distinct sections; the plasma-probe interface (generally dependent on probe geometry and plasma operating conditions), the analog detection circuit (shielded cable, bandpass filters, input amplifier), and the digital processing circuit which accounts for digital effects on data acquisition and analysis via the transfer function $H_D(\omega)$. The plasma-probe interface is essentially a signal driver with voltage source $\phi(t)$ (representing probe floating potential fluctuations) and output impedance $Z_p(v_0, \omega)$ (the plasma-probe sheath impedance where v_0 is the static sheath potential drop). Assuming constancy of electron temperature over a signal acquisition period, $\phi(t)$ is equivalent to local plasma potential fluctuations. The analog circuit is characterized by an effective input or driving point impedance $Z_i(\omega)$ and potential transfer function $H_c(\omega)$. From equation 15, the net analog detected signal is therefore:

$$\phi^{A}_{DET}(t) = \frac{1}{2\pi} \int_{-\infty}^{\infty} H(\omega)\Phi(\omega)e^{-i\omega t}d\omega \qquad (19)$$

where the composite analog transfer function is:

$$H(\omega) = \left[\frac{Z_i(\omega)}{Z_p(v_0,\omega)+Z_i(\omega)}\right] H_c(\omega) \qquad (20)$$

$Z_i(\omega)$, $H_c(\omega)$ and in principle $Z_p(v_0,\omega)$ are all experimentally measurable quantities. For transient plasmas where direct measurement of $Z_p(v_0,\omega)$ is possibly untenable, a semi-quantitative expression is derivable from basic plasma considerations as follows.

The total plasma current density drawn by an electrostatic probe as a function of probe bias is:

$$J_T(v) = J_p(v) + \frac{1}{4\pi}\frac{\partial}{\partial t} E_p(v) \tag{21}$$

where $v(t)$ represents probe bias with respect to the plasma potential (i.e., the probe sheath potential drop), $J_p(v)$ and $E_p(v)$ represent the collected current density and electric field at the probe surface as a function of bias respectively, and $\frac{1}{4\pi}\frac{\partial}{\partial t} E_p(v)$ defines the displacement current contribution due to temporal space charge changes in the probe sheath. The sheath potential drop may be further dichotomized into a static and fluctuating component:

$$v(t) = v_0 + \phi(t) \tag{22}$$

yielding a Taylor series expansion of $J_T(v)$ about v_0:

$$J_T(v) = J_p(v_0) + j_T(\phi) \tag{23}$$

where:

$$j_T(\phi) = \left.\frac{\partial J_T(v)}{\partial v}\right|_{v_0} \phi(t) = \left[\left.\frac{\partial J_p(v)}{\partial v}\right|_{v_0} + \frac{1}{4\pi}\frac{\partial}{\partial t}\left.\frac{\partial E_p(v)}{\partial v}\right|_{v_0}\right]\phi(t) \tag{24}$$

Fourier Transforming (23) yields:

$$J_T(v_0,\omega) = J_p(v_0) + j_T(\omega) \tag{25}$$

where

$$j_T(\omega) = \left.\frac{\partial J_p(v)}{\partial v}\right|_{v_0}\left[1 + \frac{i\omega}{4\pi}\left.\frac{\partial E_p(v)}{\partial J_p(v)}\right|_{v_0}\right]\Phi(\omega) \tag{26}$$

For an ion attracting probe, the probe-plasma sheath is primarily dominated by positive space charge and hence, the dependence of collected current density on sheath electric field (Equation 26) is essentially determined by space charge limited ion flow. For the case of a planar probe, or cylindrical or spherical probe operating in the thin sheath limit [26], collected ion current density is approximately given by the Child-Langmuir relation:

$$J_i(v) = \frac{4}{9}\left(\frac{2q_i}{M_i}\right)^{1/2}\frac{v^{3/2}}{4\pi d^2} \tag{27}$$

where d is the probe sheath thickness. Defining $E_p(v) \sim v/d$, setting v_0 at the probe floating potential, and employing equation (27) yields:

$$\left.\frac{\partial E_p(v)}{\partial J_p(v)}\right|_{v_0} \approx \frac{4\pi d}{C_s}\left[\ell n\left(\frac{M_i}{m_e}\right)\right]^{-1/2} \approx 4\pi\tau_i \tag{28}$$

where C_s is the ion sound speed ($C_s = \sqrt{T_e/M_i}$) and τ_i is essentially the mean ion transit time through the probe-plasma sheath. Although equation (28) assumes a floating probe, it is approximately correct for most of the ion attracting probe operation regime where $ev_0 >> kT_e$

since it is relatively insensitive to probe bias. By employing equations 26 and 28 , equation 25 may be cast in the form of an admittance relation:

$$I_T(v_0,\omega) = I_p(v_0) + Y_p(v_0,\omega)\Phi(\omega) \tag{29}$$

where $I_p(v_0)$ is the D.C. collected probe current at bias v_0 (zero for a floating probe); $Y_p(v_0,\omega)$, the dynamic probe sheath admittance, is defined by

$$Y_p(v_0,\omega) = Y_p(v_0)[1 + i\omega\tau_i] \tag{30}$$

and $Y_p(v_0)$, the static probe sheath admittance, is:

$$Y_p(v_0) = \left.\frac{\partial I_p(v)}{\partial v}\right|_{v_0} = \left[Z_p(v_0)\right]^{-1} \tag{31}$$

For frequencies well below the ion plasma frequency, probe sheath reactance is negligible and hence sheath admittance is determined by measuring the slope of the probe current-voltage characteristic about the static operating point. Probe sheath impedance, defined as the inverse of admittance, is therefore an easily determined quantity. Since $I_p(v)$ is a nonlinear function of sheath potential, $Z_p(v_0)$ will in in general behave like a nonlinear circuit element. Deleterious nonlinear effects in the analog detection circuit may, however, be avoided by minimizing the ratio of probe sheath to analog input impedance over the measurement bandwidth ($|Z_p(v_0)| / |Z_i(\omega)| \ll 1$). This condition must be mitigated by considerations of finite probe size since probe sheath impedance is inversely proportional to probe area. A probe of

scale length L_p will effectively act as a low pass spatial filter with cut off at $k \simeq 2\pi L_p^{-1}$. Accurate spectral measurement therefore requires that probe size remain much smaller than the fluctuation wavelength. In any case, the determination and utilization of the composite analog response function (Eq. 20) is rather straightforward.

B. Digital Effects

The preceding discussion has addressed the topic of spectral analysis from the standpoint of continuum mathematics. That is, all spectral variables were continuous functions of time or frequency. Digital data processing, however, requires all continuous functions be replaced by their discrete counterparts; since digitized quantities are only defined at a finite number of discrete sample points. This process is conceptually illustrated in Figure 4. The signal digitizer essentially multiplies the detected analog waveform by a sampling comb consisting of N samples with sampling frequency $f_s = 1/\Delta t$ and total duration $T = N\Delta t$. In addition, the signal amplitude at each sample point is quantized to a fixed number of discrete levels set by the capacity of the analog to digital converter (e.g. an eight bit ADC will allow 2^8 or 256 quantized amplitude levels). The resulting output signal is a digitized representation of the analog input waveform whose accuracy is strongly dependent on the following considerations.

Bandwidth Limitation. One consequence of the Whittaker-Shanon sampling theorem is that an infinite, but discrete time series will completely describe a continuous waveform, provided the waveform is bandwidth limited to half the discrete sampling frequency (also known

as the Nyquist frequency).[27,28] In effect, the theorem formalizes a well-known concept in information theory that the maximum rate of information transfer is proportional to the transmission bandwidth. Input signal components above the Nyquist frequency will, when sampled, be falsely interpreted as lower frequency information; an effect known as aliasing.[29] Aliasing is a straightforward consequence of sampling at equally spaced intervals and cannot be removed from the digitized data once sampling has occurred. Therefore, bandwidth limitation of the analog input is a necessity which entails passing the signal through a suitable low pass or band pass filter before digitization occurs. The effect of filter response on overall system performance is then included in the analog transfer function $H(\omega)$, previously described.

Data Window. The spectral composition of an input bandlimited signal ($|\omega| \leq 2\pi f_s$) may be expressed as an infinite Fourier series over the bandwidth interval:

$$\Phi^{A}_{DET}(\omega) = \sum_{n=-\infty}^{\infty} \phi^{A}_{DET}(t_n) e^{i\omega t_n} \tag{32}$$

where

$$\phi^{A}_{DET}(t_n) = \int_t \phi^{A}_{DET}(t)\delta(t-t_n)dt \tag{33}$$

$$= \frac{1}{2\pi f_s} \int_{-\pi f_s}^{\pi f_s} \Phi^{A}_{DET}(\omega) e^{-i\omega t_n} d\omega \tag{34}$$

and: $\phi^{A}_{DET}(t)$ represents the continuous analog input to the digital system in the notation of Figure 3.

$t_n = n\Delta t$ represents the discrete sample points where Δt is the intra-sample period and is equivalent to the inverse of the sample frequency f_s.

The act of experimental measurement, however, necessitates a finite data record and consequently, equation 32 must be modified accordingly. The digitally measured signal may be expressed in terms of the band limited input as:

$$\phi_{DET}(t_n) = \phi^{A}_{DET}(t_n)\, w_R(t) \tag{35}$$

where $w_R(t)$ defines the rectangular data window:

$$w_R(t) = \begin{cases} 1 & 0 \leq t \leq t_{N-1} \\ 0 & \text{otherwise} \end{cases} \tag{36}$$

Hence, by employing equations 32 through 36, the spectral composition of the digitized signal is given by:

$$\Phi_{DET}(\omega_m) = \sum_{n=0}^{N-1} \phi_{DET}(t_n) e^{i\omega_m t_n} \tag{37}$$

where $\Phi_{DET}(\omega_m)$ defines the discrete spectral transform of $\phi_{DET}(t_n)$ at frequencies $\omega_m = 2\pi m/N\Delta t$. Note that equation 37 is periodic with period $2\pi f_s$.

The inverse transform relation may be obtained by utilizing the orthogonal property of the complex exponentials over a set of discrete, equally spaced points covering the period:

$$\sum_{m=o}^{N-1} e^{i\omega_m(t_n-t_j)} = N\delta_{nj} \tag{38}$$

Thus, multiplying both sides of equation (37) by $e^{-i\omega_m t_j}$ and summing over m yields:

$$\sum_{m=o}^{N-1} \Phi_{DET}(\omega_m)e^{-i\omega_m t_j} = \sum_{m=o}^{N-1}\sum_{n=o}^{N-1} \phi_{DET}(t_n)e^{i\omega_m(t_n-t_j)}$$

$$= N \sum_{n=0}^{N-1} \phi_{DET}(t_n)\delta_{nj} \tag{39}$$

$$= N\phi_{DET}(t_j)$$

Hence:

$$\phi_{DET}(t_n) = \frac{1}{N} \sum_{m=o}^{N-1} \Phi_{DET}(\omega_m)e^{-i\omega_m t_n} \tag{40}$$

Again, note that equation 40 is periodic with period T (the total sample duration). Equations 37 and 40 form the discrete counterparts of the continuous spectral transforms defined by equation 3. The spectral relationship between the discrete and continuous transform relations (equations 3 and 37) may be obtained by Fourier transforming equation 35, yielding the periodic convolution:

$$\Phi_{DET}(\omega_m) = \frac{1}{2\pi f_s} \int_{-\pi f_s}^{\pi f_s} \overset{A}{\Phi}_{DET}(\omega)W_R(\omega_m-\omega)d\omega \tag{41}$$

where $W_R(\omega)$ represents the Fourier transform of the rectangular data window $w_R(t)$:

$$W_R(\omega) \approx T \frac{\mathrm{Sin}(\omega T/2)}{T/2)} e^{i\omega T/2} \qquad (42)$$

The transform $W_R(\omega)$ (Figure 5A) effectively acts like a digital transfer function ($H_D(\omega)$) relating analog to digital spectral content. Accurate spectral measurement therefore requires the main lobe width of the window function be considerably less than the inverse coherence time of the detected signal. In addition, the large sidelobe content of $W_R(\omega)$, resulting from the sharp temporal discontinuity in $w_R(t)$, effectively decreases the transform frequency resolution to something greater than the main lobe width due to the leakage of spectral information across a moderately wide frequency range. The usual approach of reducing sidelobe leakage entails utilizing a temporal data window with a less severe discontinuity and hence lower sidelobe content. One example is the Hanning window defined by:

$$w_H(t) = \frac{1}{2}\left[1-\mathrm{Cos}\left(\frac{2\pi t}{T}\right)\right] w_R(t) \qquad (43)$$

Figure 5B illustrates the spectral transform of equation 43 ($W_H(\omega)$). The main lobe is twice as wide as the corresponding rectangular window however, side lobe level and associated leakage is greatly reduced. The digital transform is again related to its continuous counterpart by the periodic convolution (equation 41):

$$\Phi_{DET}(\omega_m) = \Phi^A_{DET}(\omega) * H_D(\omega)\Big|_{\omega=\omega_m} \qquad (44)$$

where the digital transfer function is given by:

$$H_D(\omega) = W_H(\omega) \tag{45}$$

Hence, combining equation 44 with the analog response described by equation 16 yields the total system detected spectral density (Figure 3):

$$\Phi_{DET}(\omega_m) = \Phi(\omega)H(\omega)*H_D(\omega)\Big|_{\omega=\omega_m} \tag{46}$$

where $\Phi(\omega)$ represents the spectral density of the input plasma potential fluctuations $\phi(t)$, and $H(\omega)$ represents the composite analog response function defined by equation 20.

Cross Power Spectral Estimation: Substituting equation 46 into equation 9, yields the detected cross power spectrum assuming two matched channels (A and B):

$$S^{\phi}_{AB}(\vec{R},\omega_m)\big|_{DET} \approx S^{\phi}_{AB}(\vec{R},\omega)\,|H^2(\omega)|*|H^2_D(\omega)|\Big|_{\omega=\omega_m} \tag{47}$$

The measured cross power spectrum is, in actuality, a statistical estimate of the true cross power spectrum since for a finite number of data samples, statistical noise is significant. The effects of statistical noise on spectral measurement may be reduced by ensemble averaging the measurements over a series of statistically independent data sets. That is, letting $\mathrm{Re}[S^{\phi}_{AB}|_{DET}]_j$ and $\mathrm{Im}[S^{\phi}_{AB}|_{DET}]_j$ represent the real and imaginary components of the detected cross power spectrum for data set j, the ensemble averaged cross power spectral quantities are given by:[30]

$$\langle |S^{\phi}_{AB}(\omega_m)| \rangle = \frac{1}{M}\left[\left(\sum_{j=1}^{M} \mathrm{Re}[S^{\phi}_{AB}|_{DET}]_j\right)^2 + \left(\sum_{j=1}^{M} \mathrm{Im}[S^{\phi}_{AB}|_{DET}]_j\right)^2\right]^{1/2} \tag{48}$$

$$\langle \Theta_{AB}(\vec{R},\omega_m) \rangle = \mathrm{ARCTAN}\left[-\frac{\sum_{j=1}^{M} \mathrm{Im}[S^{\phi}_{AB}|_{DET}]_j}{\sum_{j=1}^{M} \mathrm{Re}[S^{\phi}_{AB}|_{DET}]_j}\right] \tag{49}$$

$$\langle \gamma^{\phi}_{AB}(\omega_m) \rangle = \frac{\langle |S^{\phi}_{AB}(\omega_m)| \rangle}{[\langle S^{\phi}_{AA}(\omega_m)\rangle\langle S^{\phi}_{BB}(\omega_m)\rangle]^{1/2}} \tag{50}$$

where M denotes the total number of data sets in the averaging ensemble. Note that the ensemble averages are performed for each of the N discrete frequencies at which the spectral quantities are defined. The statistical variance of the averaged cross power spectral quantities are given by:[30]

$$\mathrm{VAR}\,\langle |S^{\phi}_{AB}(\omega_m)| \rangle \approx \frac{1}{2M}\langle |S^{\phi}_{AB}(\omega_m)| \rangle^2 \left[1 + \frac{1}{\langle \gamma^{\phi}_{AB}(\omega_m)\rangle^2}\right] \tag{51}$$

$$\mathrm{VAR}\,\langle \Theta_{AB}(\vec{R},\omega_m)\rangle \approx \frac{1}{2M}\left[\frac{1}{\langle \gamma^{\phi}_{AB}(\omega_m)\rangle^2} - 1\right] \tag{52}$$

$$\mathrm{VAR}\,\langle \gamma^{\phi}_{AB}(\omega_m)\rangle \approx \frac{1}{2M}\left[1 - \langle \gamma^{\phi}_{AB}(\omega_m)\rangle^2\right]^2 \tag{53}$$

The statistical signal to noise ratio follows the familiar Gaussian result and increases proportional to the square root of the number of independent data sets averaged. In addition, both the cross power phase and coherence are strongly dependent on the averaged coherence spectrum.

One standard method of minimizing statistical noise entails dividing a single data record of N samples into M subsets of N/M samples each. After the application of a suitable data window to each subset, the subsets are transformed and averaged yielding reduced statistical noise at the expense of reduced transform resolution. For many applications, however, this trade off is acceptable as long as transform resolution remains significantly greater than the signal inverse coherence time.

Quantization. In addition to a finite data record, the digitized signal amplitude, represented by equation 35, is quantized to a fixed number of discrete levels by the analog to digital converter. The effects of signal quantization on spectral analysis are conceptually equivalent to the deleterious effects of coefficient quantization on the algorithm used to compute the spectral transform. Although the nature of coefficient quantization is inherently nonstatistical, a rough statistical analysis of quantization noise is possible by replacing each discrete transform coefficient (e.g. equation 37) by its true value plus a white noise source called jitter. The resulting signal to noise ratio for an FFT algorithm is approximately:[31]

$$\left(\frac{\text{Signal}}{\text{Noise}}\right)_{\text{Quantization}} \sim 6\left[\frac{2^{2b}}{\log_2 N}\right] \tag{54}$$

where b represents the number of bits available for amplitude storage in the ADC and N is the total number of points transformed. The key result of equation 54 is that the signal to noise ratio is a weak function of the total number of transformed points, but has a strong dependence on the number of quantized amplitude levels available in the ADC.

IV. EXPERIMENTAL RESULTS

Figure 6 shows computer generated plots of the cross power spectral functions defined by equations 11 through 13 under typical source plasma operating conditions. The measurements were performed with two shielded, unidirectional disk probes positioned on axis, with a relative separation of .4 cm and facing towards the gas inlet (Figure 1). Each plot represents an ensemble average over 80 data sets yielding a spectral resolution of approximately 40 kHz. Note that the variance of the spectral quantities are greatly reduced over frequency bands of high coherence as predicted by equations 51-53.

The cross power spectral density, coherence, and phase measurements indicate the fluctuations are reasonably coherent and possess a fairly linear dispersion relation (constant slope in the cross power phase plot) across the resonant spectrum (800-2000 kHz); consistant with the properties of ion acoustic fluctuations. Measured values of the propagation velocity and direction are in agreement with the hypothesis that the ion acoustic spectrum is initially excited by a current driven instability at the thermionic cathode, and subsequently modified by a positive feedback mechanism dependent on the multifilament cathode structure.[32]

CONCLUSION

The degree to which a detected spectral function approximates reality will, to a large extent, depend on a judicious choice of the analog and digital components which comprise the measurement apparatus. The preceeding discussion has briefly presented the general considerations behind successful digital spectral measurement. However, in the final analysis, the actual choice of specific system components will directly depend on properties of the spectrum under consideration.

ACKNOWLEDGEMENTS

My overall thanks to the Lawrence Berkeley Laboratory Neutral Beam Group for their general support and assistance. In particular, to W. B. Kunkel for discussions on source physics, B. D. Billard and W. F. Steele for experimental apparatus - software suggestions, G. Guethlein for experimental assistance, and M. McElhiney and A. Aitkens for manuscript processing. This work was performed under the auspices of the U. S. Department of Energy.

FOOTNOTES AND REFERENCES

† Current address: Los Alamos Scientific Laboratory, P. O. Box 1663, Los Alamos, NM 87545.

1. S. M. Hamberger and J. Jancarik; Phys. Rev. Lett. 25 (1970), 999.

2. G. S. Mills, C. K. McLane and T. Tsukishima; Phys. Fluids 13, (1970), 2135.

3. E. B. Hooper, Jr., Plasma Phys. 13 (1971), 1.

4. J. Reese Roth, Phys. Fluids 14 (1971), 2193.

5. D. B. Fenneman, M.Raether and M. Yamada; Phys. Fluids 16 (1973), 871.

6. D. E. Smith and E. J. Powers; Phys. Fluids 16 (1973), 1373.

7. E. J. Powers, Nuc. Fusion 14 (1974), 749.

8. M. Yamada and M. Raether; Phys. Fluids 18 (1975), 361.

9. D. B. Ilic, K. J. Harker, and F. W. Crawford; Phys. Lett. 54A (1975), 265.

10. M. Yamada and D. K. Owens; Phys. Rev. Lett. 38 (1977), 1529.

11. F. F. Chen, "Electric Probes," in Plasma Diagnostic Techniques (R. H. Huddlestone and S. L. Leonard, eds.), Academic Press, New York (1965), 191-195.

12. K. Bol, Phys. Fluids 7 (1964), 1855.

13. J. W. Cooley and J. W. Tukey; Math. Comput. 19 (1965), 297.

14. C. Bingham, M. D. Godfred and J. W. Tukey; IEEE Trans. on Audio and Electroacoustics AU-15 (1967), 56.

15. G. D. Bergland, IEEE Spectrum 6 (1969), 41.

16. J. W. Cooley, P. A. W. Lewis, and P. D. Welch; IEEE Trans. on Audio and Electroacoustics AU-17 (1969), 77.

17. R. C. Singleton, IEEE Trans. on Audio and Electroacoustics AU-17 (1969), 93.

18. Statistically defined as the first moment of the two-time probability distribution function.

19. For example, in the case of Brownian motion, particle momentum appears as a random temporal variable on a time scale much longer than the particle driving force correlation time.

20. When measuring a strongly excited spectrum, the delta function dependence of k in equation 14 may be broadened by non-linear coupling between modes. [See V. N. Tsytovich, Theory of Turbulent Plasma, Consultants Bureau, New York (1977).]

21. K. W. Ehlers, W. R. Baker, K. H. Berkner, W. S. Cooper, W. B. Kunkel, R. V. Pyle, and J. W. Stearns; J. Vac. Sci. Technol. 10 (1973), 922.

22. L. D. Landau and E. M. Lifshitz, Statistical Physics, Pergamon, New York (1976), 384-391.

23. R. O. Lane, N. F. Morehouse, Jr., and D. L. Phillips; Nuclear Instruments and Methods 9 (1960), 87-91.

24. B. R. Hunt, IEEE Trans. on Computers, Vol. C-22 9 (1973), 805.

25. A. V. Oppenheim and R. W. Schafer, Digital Signal Processing, Prentice-Hall, New Jersey (1975).

26. K. F. Schoenberg, Rev. Sci. Instrum. 49 (1978), 1377.

27. E. T. Whittaker, Proc. Roy. Soc. Edinburgh, Sect. A, 35 (1915), 181.

28. C. E. Shannon, Proc. IRE, 37 (1949) 10.

29. R. W. Hamming, Numerical Methods for Scientists and Engineers, McGraw-Hill, New York (1973).

30. G. M. Jenkins and D. G. Watts, Spectral Analysis and Its Applications, Holden-Day, Inc., San Francisco (1968).

31. C. J. Weinstein, IEEE Trans. on Audio and Electroacoustics AU-17 (1969), 153-157.

32. K. F. Schoenberg and W. B. Kunkel; Bull. Am. Phys. Soc. 24 (1979)

FIGURE CAPTIONS

Figure 1. Cross sectional schematic of the 10 ampere source.

Figure 2. Digital spectral analysis schematic.

Figure 3. Response schematic of the spectral analysis system.

Figure 4. Conceptual illustration of signal digitization.

Figure 5. Digitization window transforms.

A) Rectangular window.

B) Hanning window.

Figure 6. Computer generated cross power spectral functions with 40 kHz resolution.

A) Cross power spectral density.

B) Cross power spectral coherence.

C) Cross power spectral phase.

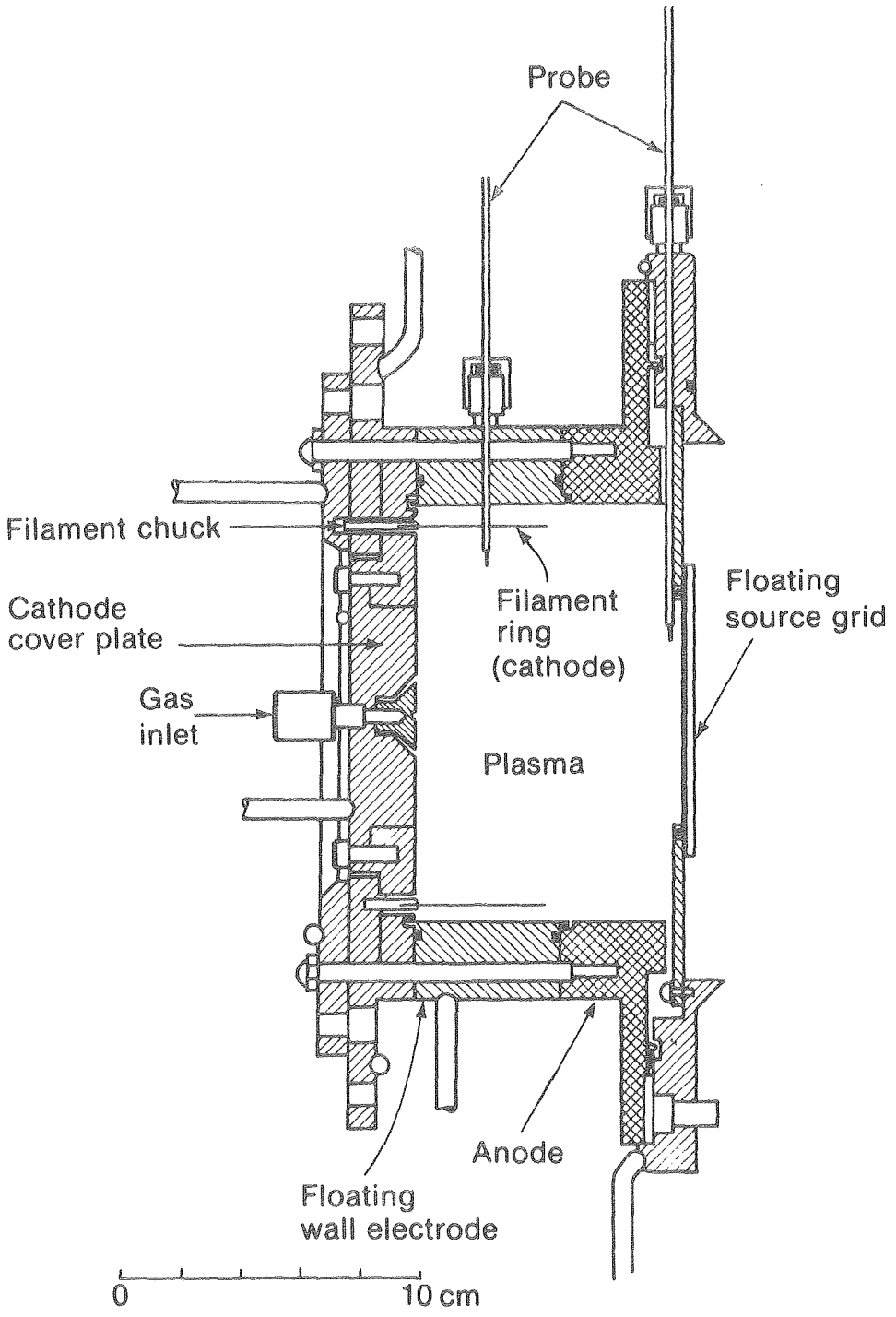

XBL 782-279

Fig. 1

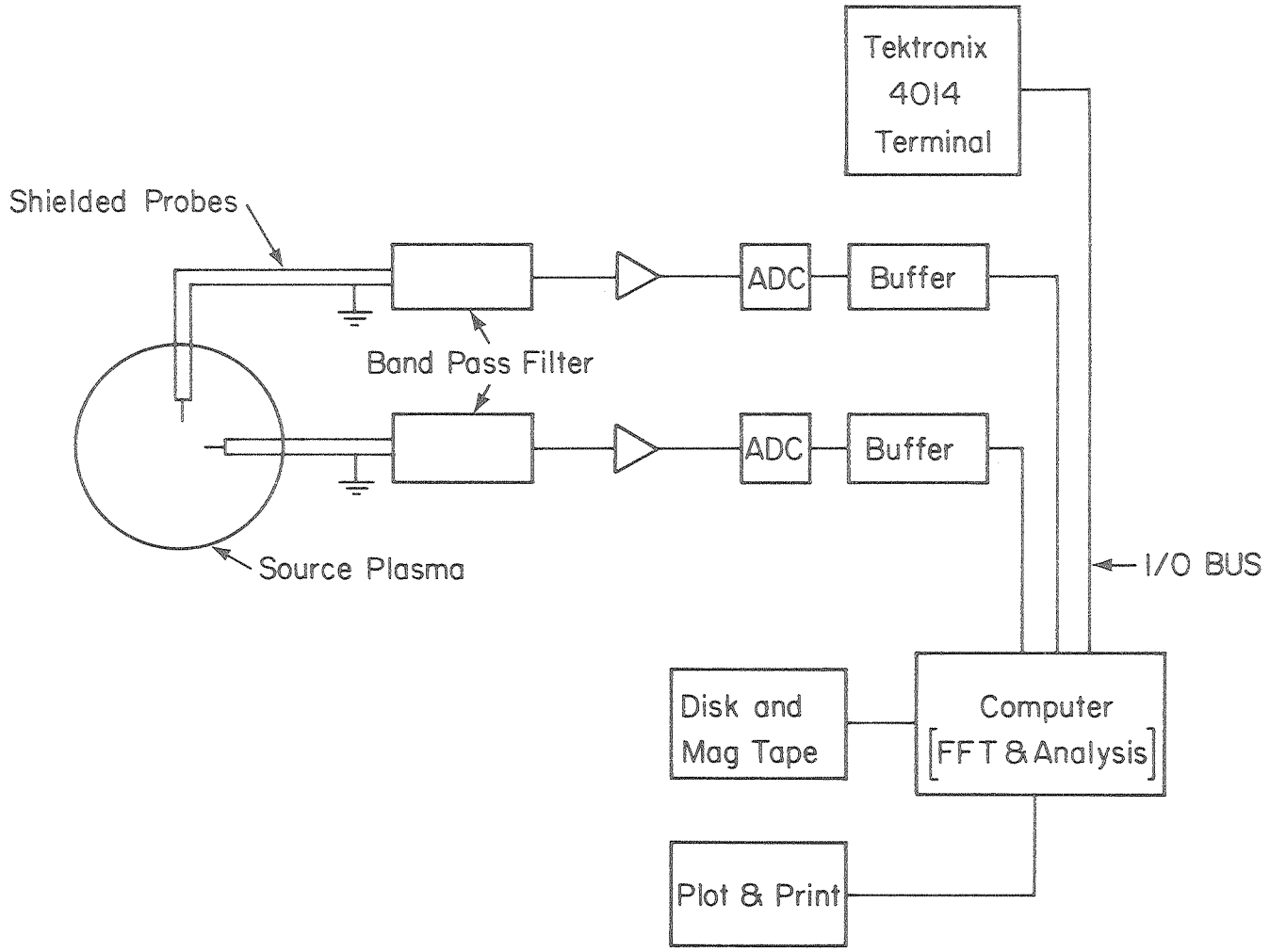

XBL 797-2327

Fig. 2

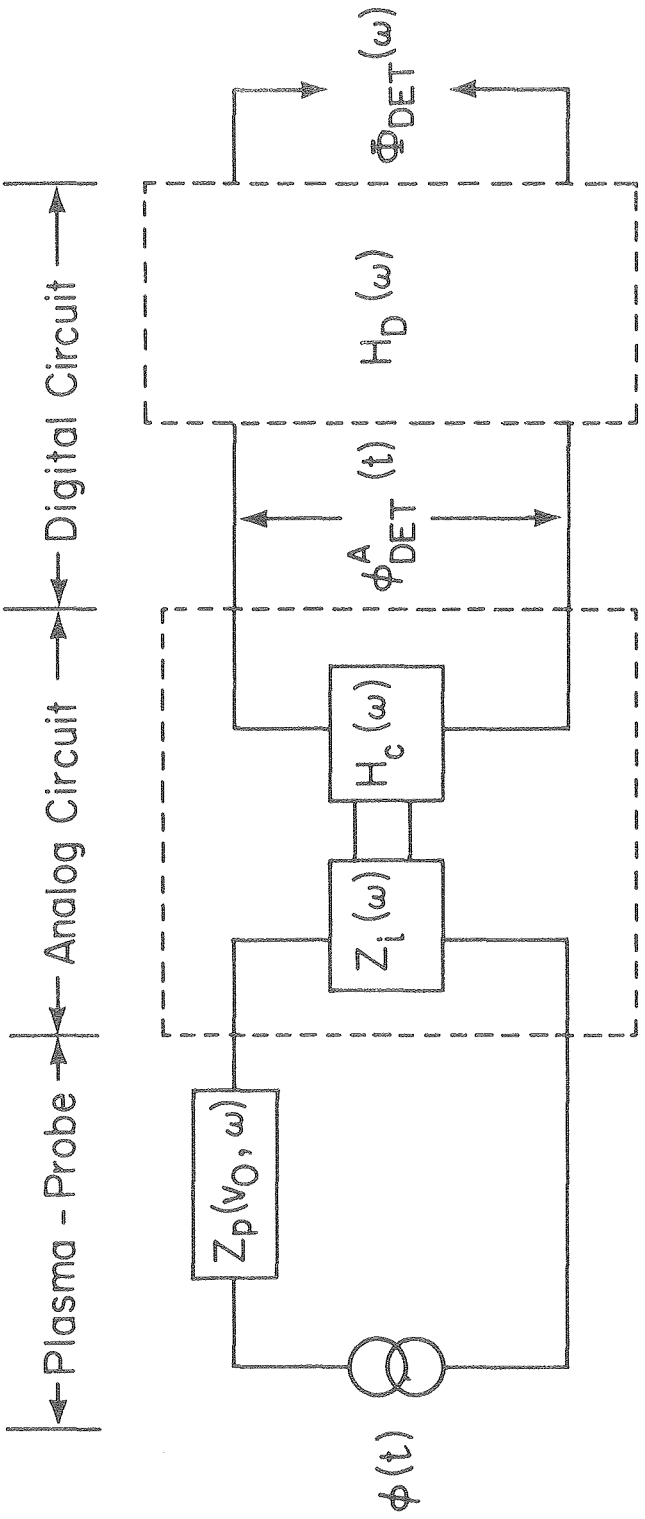

XBL 797-2328

Fig. 3

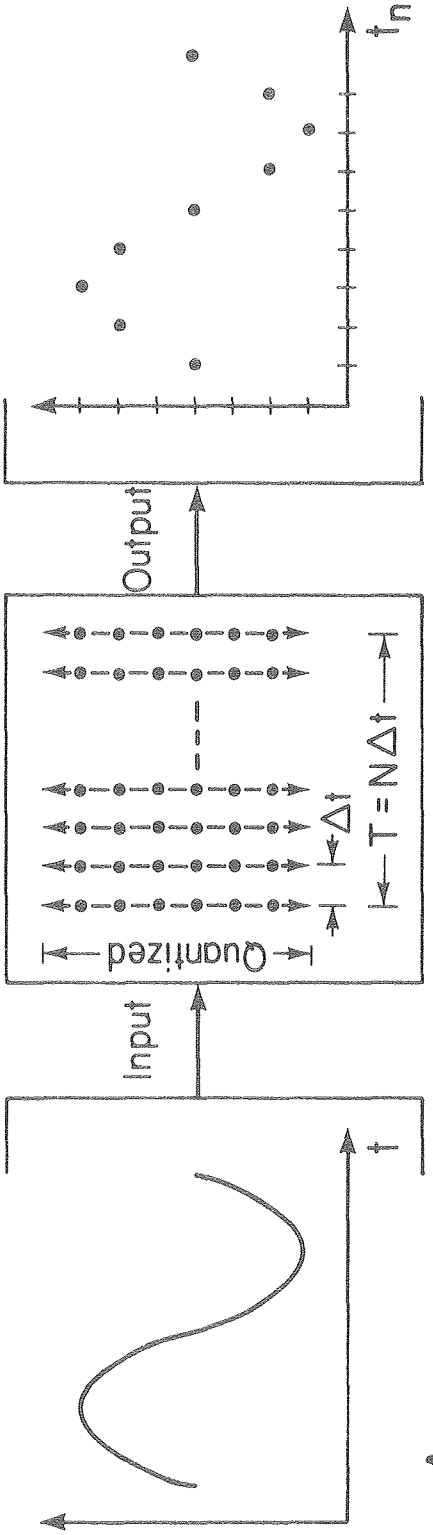

XBL 798-2654

Fig. 4

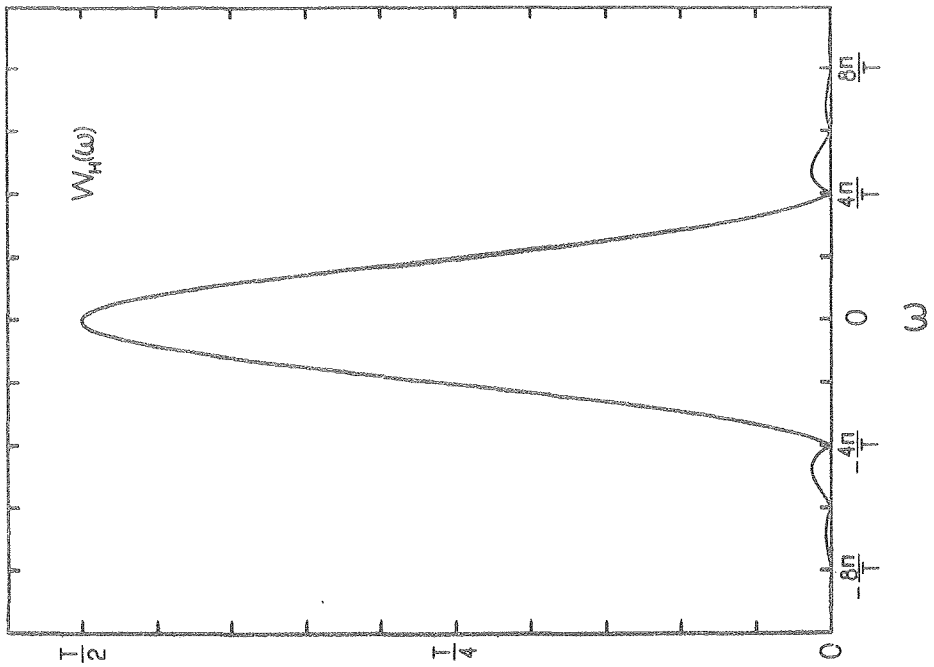

XBL 798-11009

Fig. 5B

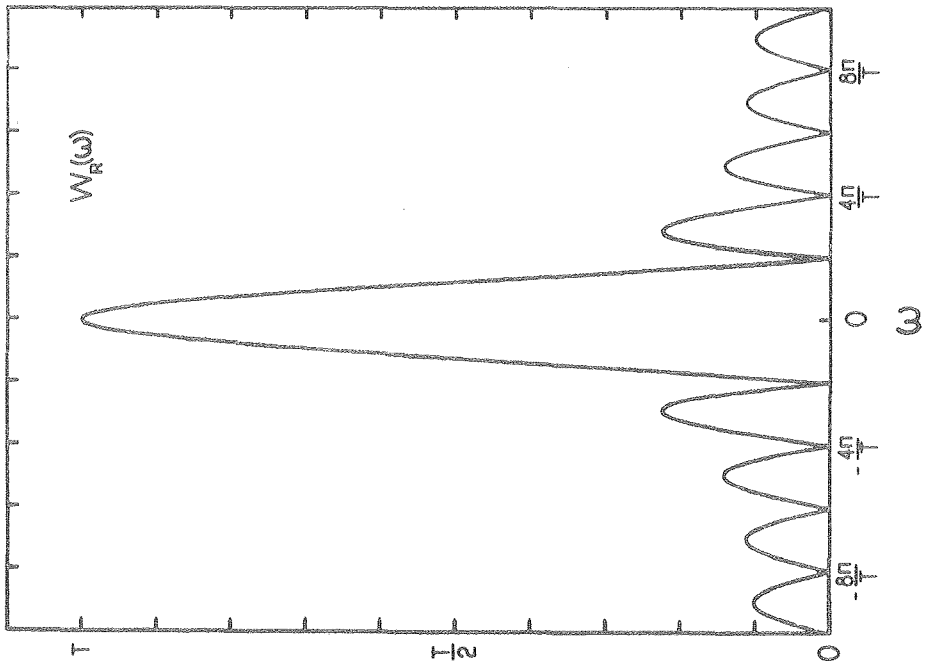

Fig. 5A

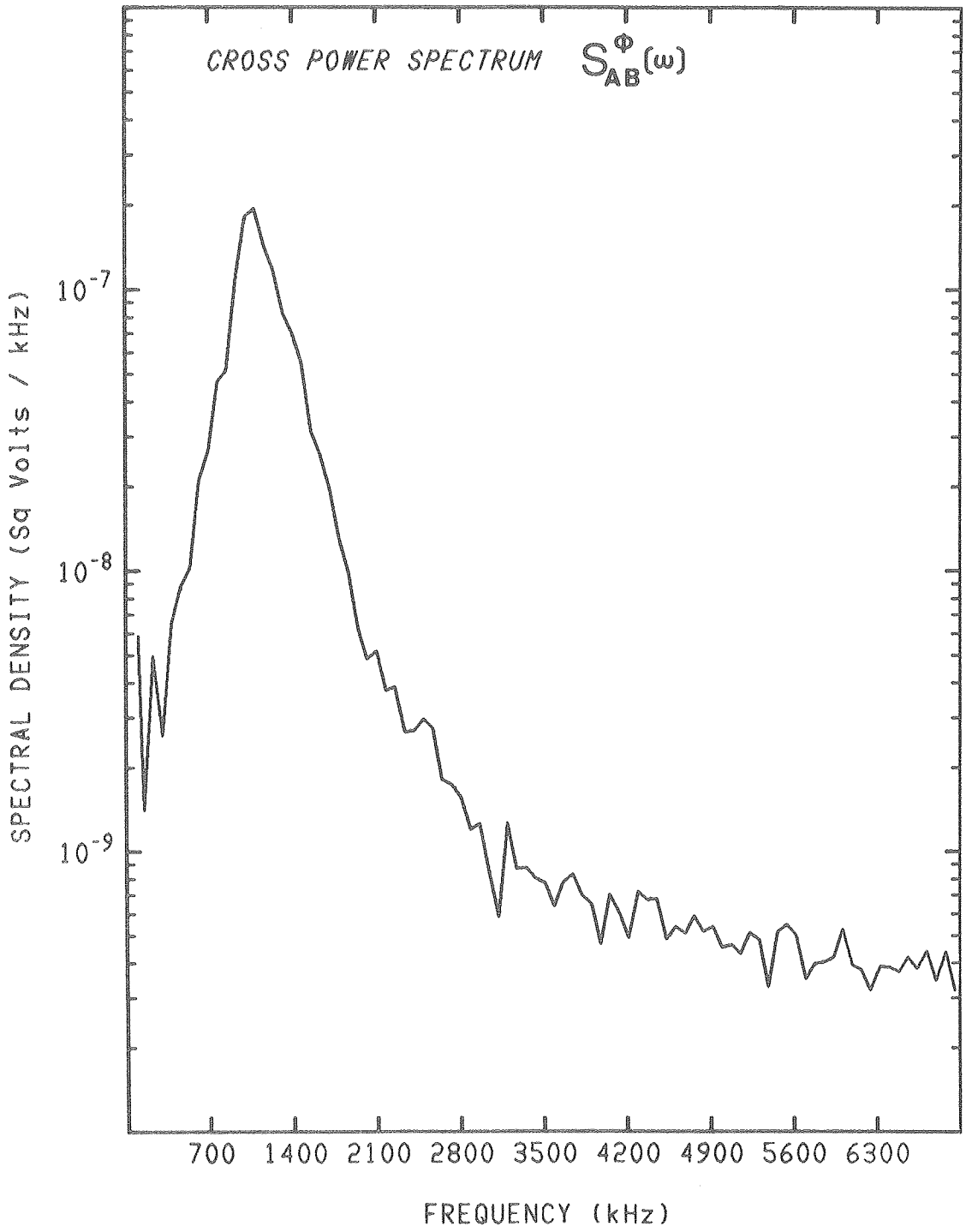

XBL 799-11644

Fig. 6A

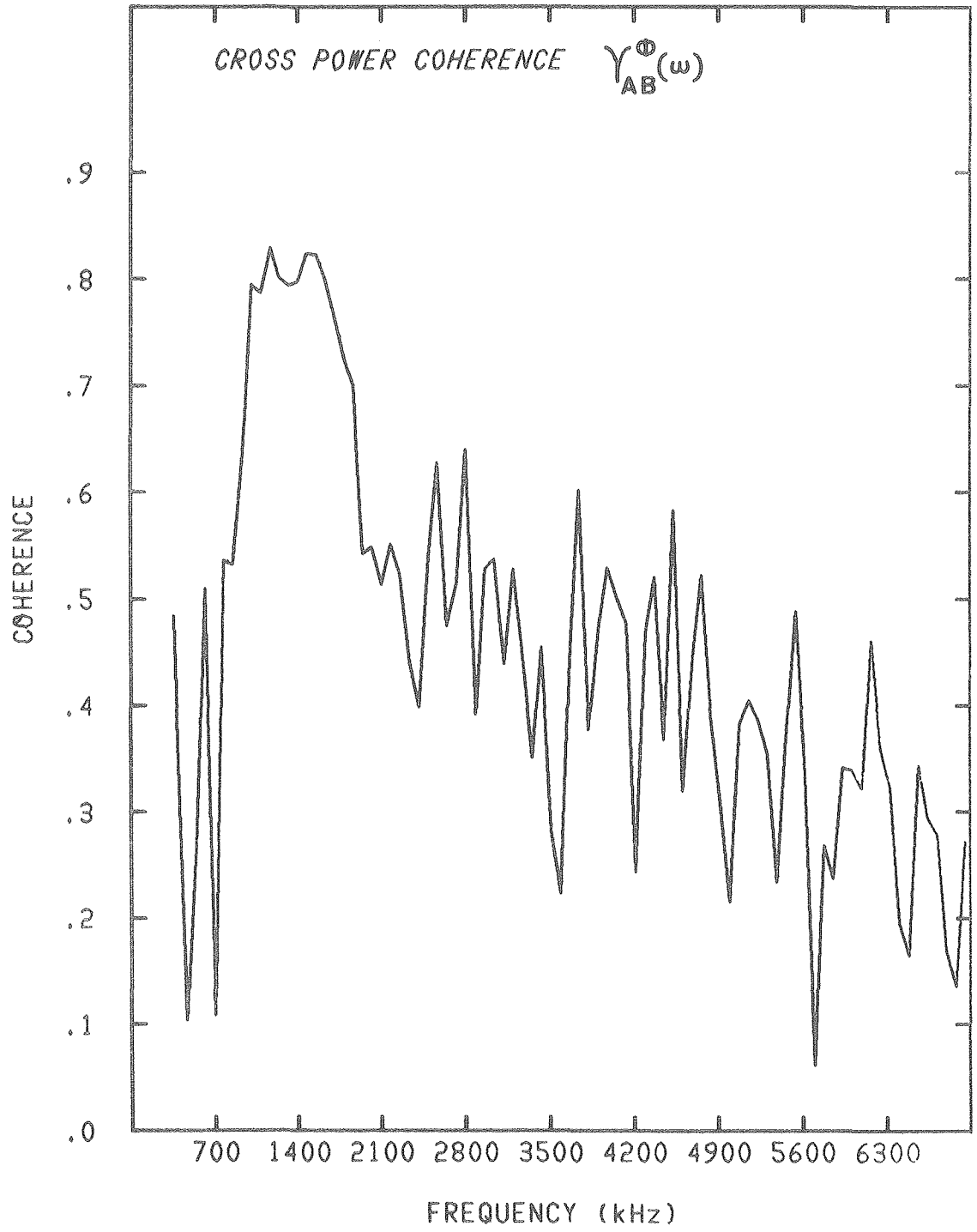
CROSS POWER COHERENCE $\gamma^{\Phi}_{AB}(\omega)$
COHERENCE
.0
.1
.2
.3
.4
.5
.6
.7
.8
.9
700 1400 2100 2800 3500 4200 4900 5600 6300
FREQUENCY (kHz)
XBL 799-11693

Fig. 6B

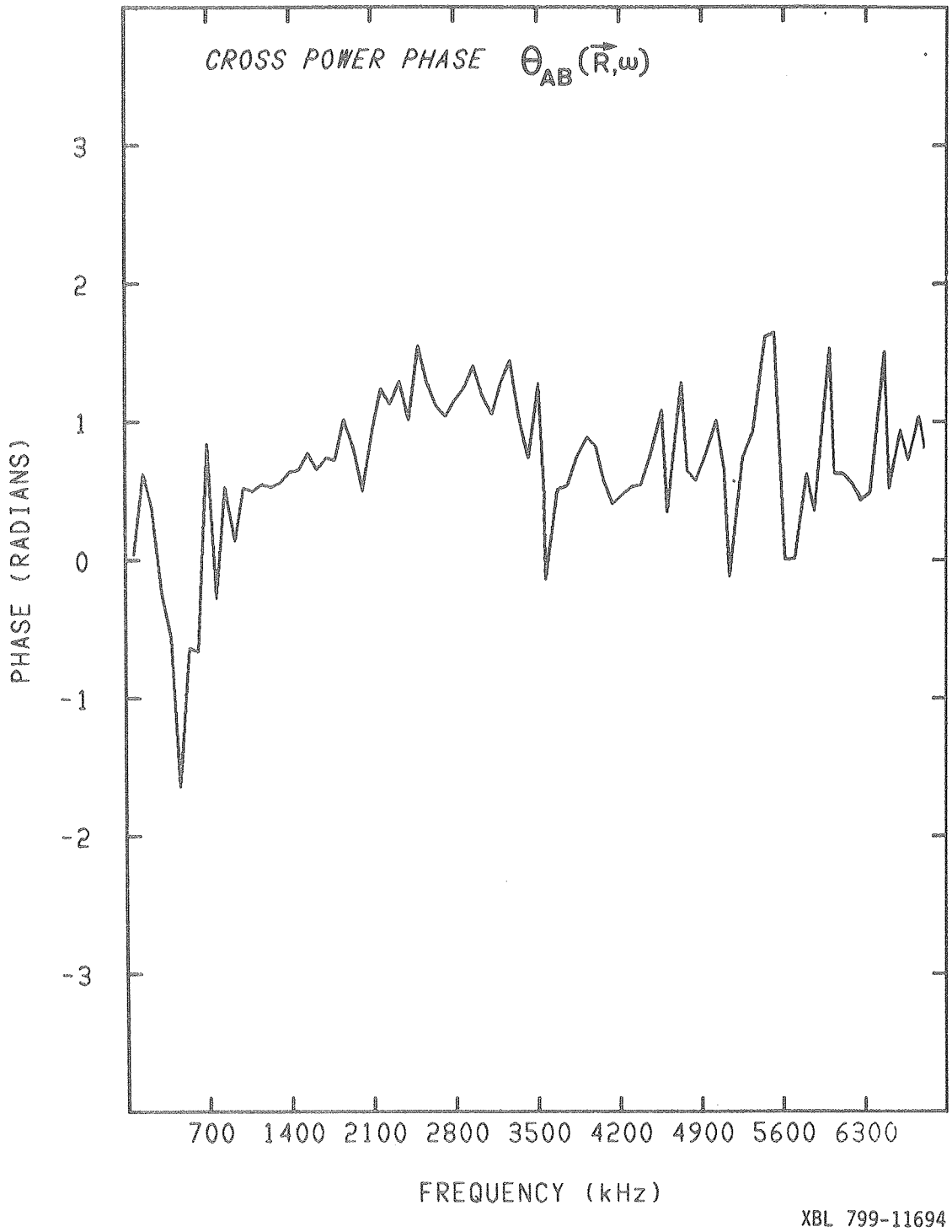
CROSS POWER PHASE $\Theta_{AB}(\vec{R},\omega)$
PHASE (RADIANS)
3
2
1
0
-1
-2
-3
700 1400 2100 2800 3500 4200 4900 5600 6300
FREQUENCY (kHz)
XBL 799-11694

Fig. 6C